May 2026

AXOL

iPSCs and New Approach Methodologies (NAMs)

Physiologically relevant *in vitro* models

Technology journal II

A highly reproducible and precise measurement platform for 3D engineered cardiac muscle tissue contractility

Svetlana Pasteuning[1] (svetlana.pasteuning@optics11life.com), Tom Berkers[1], Giulia Pilia[1], Elizaveta Loseva[1], Thorsten Jonas[1], Eliano dos Santos[2], Katarzyna Kmiotek-Caller[2], Ravi A. Kumar[2], Anna Zoccarato[2]
1 Optics11 Life, Amsterdam, The Netherlands ,2 School of Cardiovascular & Metabolic Medicine and Science, King's College London, British Heart Foundation Centre of Excellence, United Kingdom

Abstract

Engineered heart tissues (EHTs) offer more predictive insights into cardiac function than traditional 2D models but are often limited by reproducibility and scalability. Using Cuore, a 3D contractility platform from Optics11 Life, we established a robust workflow for generating consistent 3D EHTs from human Axol's iPSC-derived ventricular cardiomyocytes and cardiac fibroblasts. The platform enables controlled culture, pacing, and real-time force measurement with nanonewton sensitivity (Figure 1). Tissues show stable maturation and respond sensitively to isoprenaline, confirming reliable detection of functional drug effects. Cuore provides a scalable, high-fidelity solution for human-relevant cardiac drug testing.

Methods

Human EHTs were generated by combining 70% human iPSC-derived ventricular cardiomyocytes from Axol with 30% primary cardiac fibroblasts in a hydrogel matrix to form 3D tissue bundles. Constructs were cast into the 24-well plate Cuore platform (Figure 2), enabling controlled culture conditions and real-time functional assessment. Tissues were maintained for 42 days with daily medium changes and daily longitudinal monitoring. Contractile function of the EHTs was assessed by measuring spontaneous force of contraction, beating frequency, contraction and relaxation kinetics. At the end of the experiment, tissues were challenged with isoprenaline and β1- and β2-adrenergic receptor antagonists, followed by fixation for downstream marker stainings. The tissues were stained with DAPI, Troponin, and Vimentin (Figure 3).

- Autoclavable & Reusable
- Absolute force readout with nN and ms precision
- Integration of electrical stimulation
- Automated analysis software
- Compatible with imaging

Figure 1: Cuore platform is designed to integrate long-term culturing of 3D engineered muscle tissue, with its electrical stimulation and contractility measurements enabling a broad range of assays.

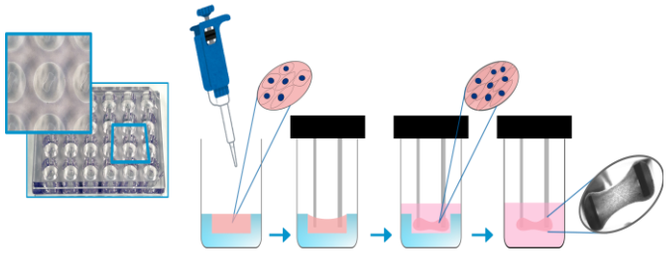

Figure 2: Cast cells embedded in hydrogel into the 24-well plate mold (*left*) and insert the cantilevers in the mixture. Cells and matrix compact around the cantilevers into a 3D tissue that can be transferred to a standard 24-well plate (*right*)

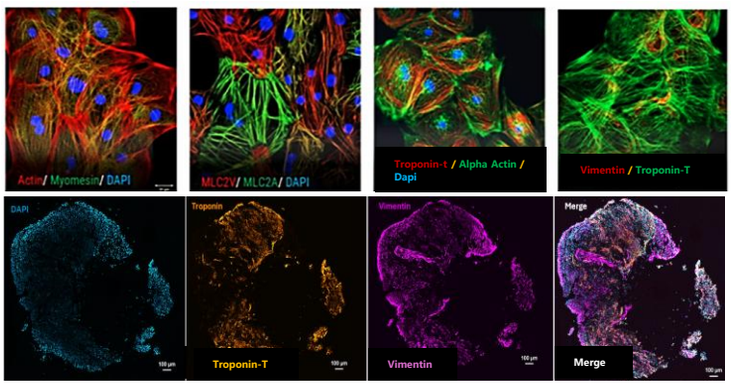

Figure 3: **(A)** 2D characterization of Axol AX2508 Ventricular Cardiomyocytes. **(B)** 3D Characterization of the casted Cardiomyocyte bundle, 30µm slice through tissue bundle – indicating healthy casted cells at Day 45 post plating.

Results

Immunostaining with DAPI, Troponin, and Vimentin revealed well-organized, healthy tissue bundles (Figure 3). No signs of necrosis or tissue damage were observed, supporting the overall robustness and physiological relevance of the model. Engineered heart tissues demonstrated progressive functional maturation over the 42-day culture period, characterized by an increase in force of contraction and spontaneous beating frequency (Figure 4A-B) and faster contraction and relaxation time and velocity (Figure 4C-D). Tissues remained viable and functional throughout the entire duration, indicating long-term stability of the model. Pharmacological stimulation with isoprenaline induced a clear dose-dependent increase in force of contraction under paced (1.5 Hz) and non-paced conditions (Figure 5A). This effect was effectively blocked by commercially available β1 (ICI189)- and β2 (ICI118)-adrenergic receptor antagonists, confirming pathway-specific responsiveness (Figure 5B).

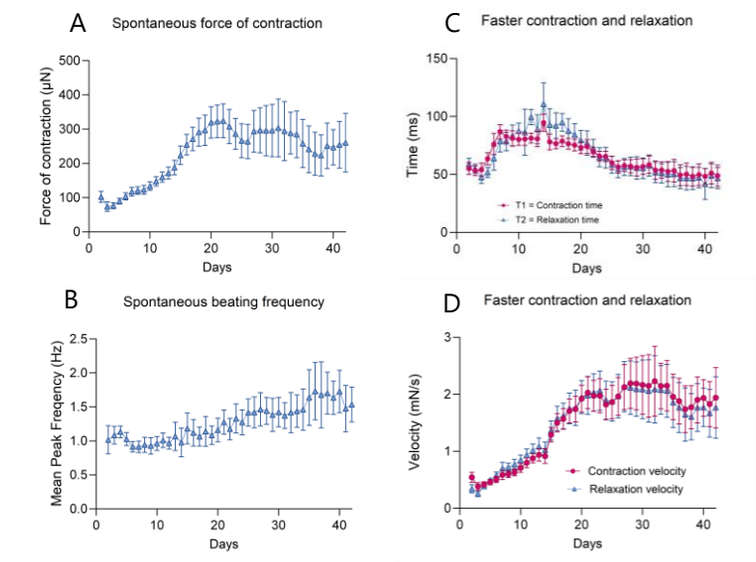

Figure 4. Maturation of EHT leads to stronger and faster contractile behavior. The Cuore system enables long-term tracking of force development over 42 days (n = 24; error bars represent standard deviation).
(A) Spontaneous force of contraction increases over time, indicating progressive tissue maturation and improved mechanical performance.
(B) Spontaneous beating frequency also rises, reflecting enhanced electrical activity and synchronization.
(C) Contraction (red) and relaxation (blue) times decrease, showing that the tissue contracts and relaxes more rapidly as it matures.
(D) Contraction and relaxation velocities increase, calculated as $V=\frac{F80\%-F20\%}{t80\%-t20\%}$, faster force generation and decay. Overall, these changes demonstrate that EHT becomes more functionally mature, with greater force output and improved contraction kinetics over time.

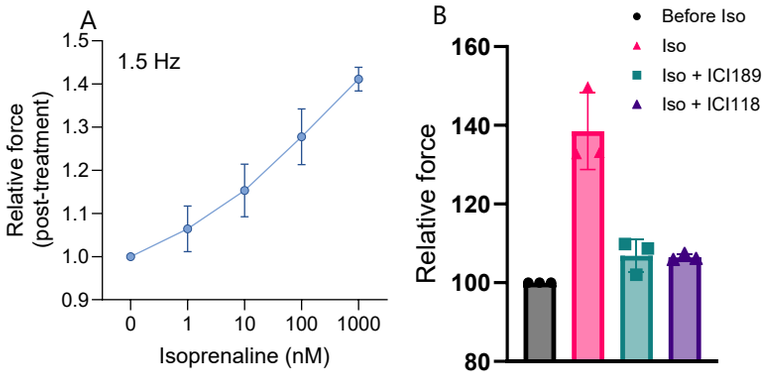

Figure 5 shows EHTs respond to pharmacological stimulation. The Cuore system measures drug-induced changes in contractility (n = 3–4; error bars indicate standard deviation).
(A) At a pacing rate of 1.5 Hz, isoprenaline (Iso) induces a dose-dependent increase in contractile force, confirming β-adrenergic responsiveness.
(B) The Cuore system detects acute drug effects from both β-receptor agonists and antagonists. Force values are normalized to baseline measurements before Iso treatment. Administration of 100 nM Iso increases contractile force, but co-treatment with 10 µM ICI189 (β1-antagonist) or ICI118 (β2-antagonist) blocks this increase, indicating receptor-specific modulation. Overall, EHTs demonstrate physiologically relevant pharmacological responsiveness.

Conclusion

These results demonstrate that the Cuore platform enables the generation of stable, functionally maturing engineered heart tissues with reliable contractile readouts over extended culture periods. Cuore's non-invasive, real-time force measurement with nanonewton sensitivity, combined with controlled pacing and multi-well scalability, enables standardized, reproducible assay conditions. The tissues exhibit physiologically relevant, dose-dependent pharmacological responses that can be specifically modulated via β-adrenergic pathways. Combined with healthy tissue structure and absence of damage, this supports the robustness and reproducibility of the model. Together, Cuore – a 3D muscle contractility platform and Axol's hiPSC-derived cardiomyocytes provide a commercially ready, end-to-end solution that aligns with New Approach Methodologies (NAMs) by enabling human-relevant, predictive, and animal-free cardiac efficacy and safety drug testing.

Functional profiling of human iPSC-derived neuronal networks with 3Brain's CorePlate™ HD-MEA technology

Ivan Verduci
3Brain IT SRL | V.le Brigate Partigiane, 14/3-4, 16129, Genova, Italy

Abstract

Functional neuronal networks derived from human iPSC-based cell types provide a powerful platform for studying synaptic development, network maturation, and pharmacological responses. This study presents the electrophysiological profiling of axoCells™ cortical excitatory neurons co-cultured with axoCells™ astrocytes, recorded on 3Brain's CorePlate™ HD-MEA system. Leveraging high-resolution sensing and integrated BrainWave6 analysis, we highlight robust, reproducible maturation and clear responses to excitatory and inhibitory modulators. Together, these results demonstrate a sensitive, reproducible, and assay-ready *in vitro* model ideally suited for neuroscience research and drug screening.

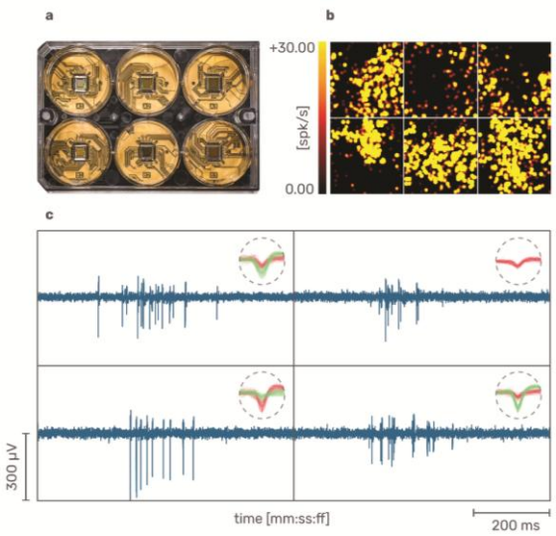

Figure 1. a) CorePlate™ 6W 38/60. b) Mean firing rate map and c) raw traces from the co-culture, illustrating spontaneous network activity. Inserts show spike-sorted waveforms obtained using BrainWave6

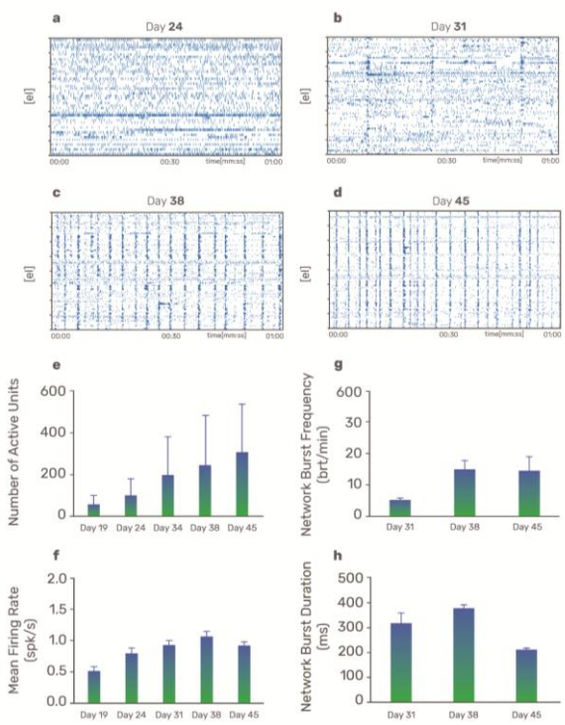

Figure 2. a-d) Raster plots of the co-culture at different maturation stages, showing the emergence of network bursts around Day 31 and their consolidation over time. e-h) Quantification of maturation metrics: active units, mean firing rate, network burst frequency, and duration.

Methods

Cell Culture

ax0015 Neural Stem Cells were cultured on Poly-D-lysine and Axol SureBond-XF-coated CorePlate™ devices. At Day 19, ax0665 human iPSC-derived astrocytes were added at an 8:1 neurons-to-astrocytes ratio to support network development.

Electrophysiological Recordings

Electrophysiological activity was recorded using the 3Brain HyperCAM Alpha platform with CorePlate 6W 38/60, featuring 13,824 simultaneously active electrodes (2,304 per well) arranged within a 2.9 × 2.9 mm^2 active area (21 × 21 µm electrodes, 60 µm pitch). Signals were sampled at 10 kHz with a 100 Hz high-pass filter and acquired longitudinally from Day 19 to track network maturation.

Pharmacological Assay

5 µM AMPA + 5 µM NMDA or 10 µM NBQX + 50 µM AP5 were used to modulate electrical activity.

Analysis Software

Data were analyzed in BrainWave6, extracting spikes and network burst metrics, raster plots, connectivity maps, and CAT analysis within a unified, fully integrated workflow.

Results

Longitudinal recordings revealed a clear progression of network development from Day 24 to Day 45, with early sparse spikes giving way to coordinated network bursts by Day 31 and further consolidation at Days 38 and 45 (Figure 2a-d). Quantitative metrics as number of active units, mean firing rate, network burst frequency, and network burst duration confirmed the maturation (Figure 2e-h). Mean firing rate map and raw-trace snapshots from Day 45 (Figure 1b-c) illustrate the spontaneous activity of fully developed networks. At this mature stage, cultures exhibited reproducible baseline firing patterns (Figure 3a). AMPA+NMDA increased excitability, enhancing spiking and network burst rates and reducing inter-spike intervals (Figure 3b-e), accompanied by broader, less clustered connectivity (Figure 4a-b). Conversely, NBQX+AP5 suppressed activity, eliminating synchronicity (Figure 3b-e) and increasing local clustering (Figure 4a-b). CAT trajectories mirrored these effects, with activation broadening propagation and blockade abolishing it (Figure 4c-d), demonstrating robust, predictable responses suitable for mechanistic and pharmacological evaluation.

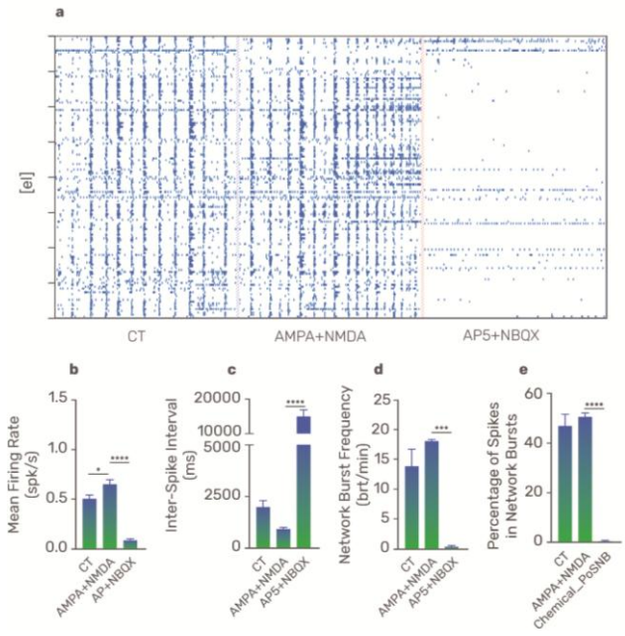

Figure 3. a) Raster plots of the co-culture at Day 45 under control conditions, after AMPA+NMDA, and after NBQX+AP5 treatment. b-e) Mean firing rate, inter-spike interval, network burst frequency, and percentage of spikes in network bursts across conditions.

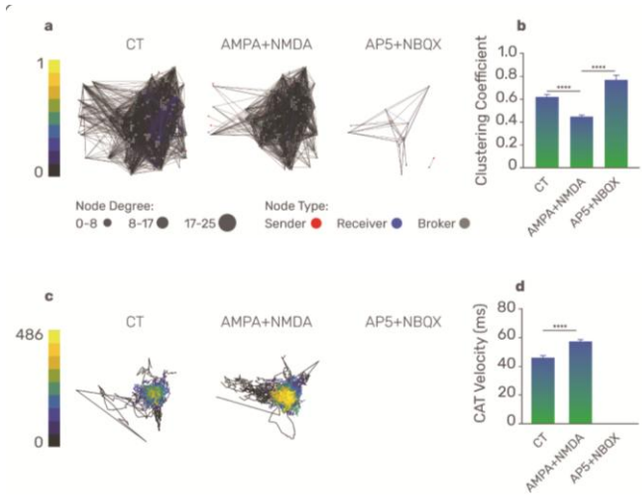

Figure 4. a) Cross-correlation maps showing connectivity changes under excitatory modulation. b) Clustering coefficient across conditions, with activation reducing clustering and blockade increasing it. c) Center of Activity Trajectories (CATs) before and after treatment. d) CAT velocity, increased by activation and reduced by blockade.

Conclusion

The findings from this study highlight the complementary strengths of Axol's human iPSC-derived neuronal biology and 3Brain's CorePlate-enabled HD-MEA technology in resolving the functional properties of cortical excitatory networks. axoCells™ Cortical Excitatory Neurons co-cultured with axoCells™ Astrocytes showed clear and reproducible maturation signatures, developing stable, synchronized activity and predictable responses to excitatory modulation, demonstrating their suitability for mechanistic studies and pharmacological evaluation.

By leveraging 3Brain's CMOS-based HD-MEA platform, 13,824 simultaneously recording electrodes across the six-well format, we achieved high-resolution mapping of network behavior, capturing both large-scale population dynamics and subtle changes arising during maturation or after pharmacological intervention. This spatial resolution supported detailed assessment of connectivity, network propagation, and activity distribution.

The integration with BrainWave 6, a unified environment for acquisition, visualization, and advanced analysis, ensured a coherent and reproducible workflow, enabling complex metrics and spatiotemporal insights without external tools.

Together, the Axol-3Brain system provides a sensitive, high-resolution, and efficient platform for neuropharmacology, toxicity testing, and the study of human neuronal circuit function.

Profiling ALS variants and ion channel expression changes with HT automated patch clamp

Nina Brinkwirth, Alison Obergrussberger, Nadine Becker, Elena Dragicevic, Niels Fertig
Nanion Technologies GmbH, Ganghoferstr 70A, Munich, Germany

Abstract

Amyotrophic lateral sclerosis (ALS) is a progressive neurodegenerative disease resulting in motor neuron loss, muscle weakness, paralysis, and death. While most cases are sporadic, over 40 genes are implicated, and mechanisms remain unclear, highlighting the need for relevant New Approach Methodologies (NAMs) and human models. Here, we functionally characterized ion channel properties of axoCells™ human iPSC-derived motor neurons from unaffected donors and C9orf72 ALS patients using the SyncroPatch 384. We observed clear differences in potassium and sodium channel properties, current densities, and neurotransmitter responses, demonstrating the value of combining iPSC-derived motor neurons with automated patch clamp for high-throughput ALS phenotyping.

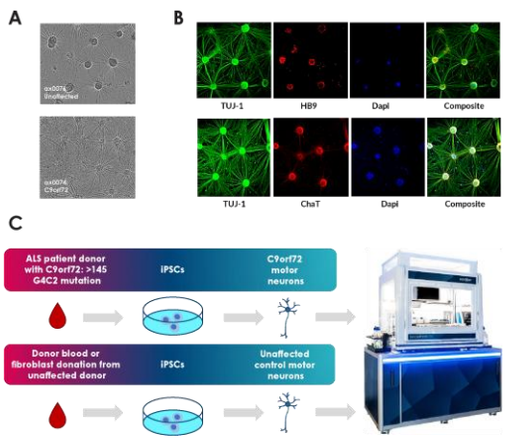

Figure 1: A At DIV10, unaffected motor neurons formed large, uniform clusters, whereas C9orf72 motor neurons showed smaller, dispersed clusters with thinner cabling and fibrous neurites. **B** Motor neuron identity was confirmed by TUJ-1, HB9/ChAT, and Isl-1 expression. **C** HTS automated patch clamp. The SyncroPatch 384 was used for recording the motor neurons with high success rates (in the GΩ range) and comparable seal resistances between the groups.

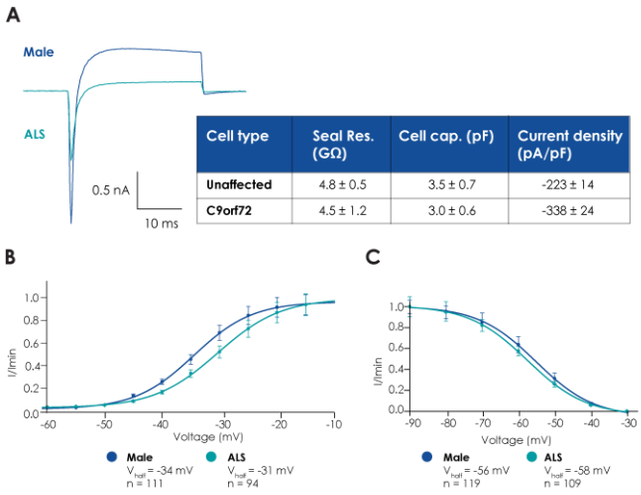

Cell type	Seal Res. (GΩ)	Cell cap. (pF)	Current density (pA/pF)
Unaffected	4.8 ± 0.5	3.5 ± 0.7	-223 ± 14
C9orf72	4.5 ± 1.2	3.0 ± 0.6	-338 ± 24

Figure 2: **A** Amplitudes and success rates of sodium (Na^+) currents were compared over a single experimental day. Na^+ current amplitudes were significantly reduced in C9orf72 motor neurons (green) compared with unaffected motor neurons (male; blue)($p < 0.001$). **B** sodium channel activation (Vhalf_act) and **C** inactivation (Vhalf_inact) parameters were comparable between the two groups.

Methods

axoCells™ human iPSC-derived motor neurons from an unaffected donor and a C9orf72 ALS patient (Axol Bioscience) were used. Cells were generated via Sendai virus reprogramming and cultured in axoCells™ maintenance media with supplements. After thawing, cells were maintained under standard conditions, becoming assay-ready ~10 days post-thaw, with maturation up to 120 days. Identity was confirmed by immunocytochemistry (TUJ-1, HB9, ChAT, Isl-1). Functional electrophysiology recordings were performed using the high-throughput automated patch clamp (APC) system, the SyncroPatch 384 (Nanion Technologies). Cells were recorded in whole-cell mode, enabling parallel analysis of up to 384 cells. Sodium and potassium currents were recorded, and neurotransmitter responses were assessed, with both cell types measured on the same chip for direct comparison.

Results

axoCells™ iPSC-derived motor neurons from an unaffected donor (Male) and a C9orf72 ALS patient (ALS) were characterized using the SyncroPatch 384. At DIV10, brightfield imaging revealed clear morphological differences (Fig. 1A). Motor neuron identity was confirmed by high expression of TUJ-1, HB9, ChAT, and Isl-1 (Fig. 1B). High-quality whole-cell recordings with consistently high seal resistances were achieved across both cell types, enabling robust and reproducible comparisons. C9orf72 neurons exhibited significantly reduced Na^+ current amplitudes compared to controls, while voltage-dependent activation and inactivation parameters remained unchanged, indicating preserved channel gating but altered channel expression or membrane properties (Fig. 2A,B,C). K^+ current analysis revealed pronounced functional remodeling. Unaffected motor neurons exhibited fast activation with pronounced inactivation, characteristic of transient outward K^+ currents (I_A). In contrast, C9orf72 motor neurons displayed sustained currents with little or no inactivation, consistent with delayed rectifier K^+ currents (I_K) (Figure 3A,B). These changes were accompanied by significantly reduced current amplitudes and current density, as well as a shift in waveform distribution, indicating altered channel composition and repolarization dynamics (Fig. 3A,C). Neurotransmitter profiling further highlighted disease-relevant alterations. While glutamate-evoked responses showed no differences in amplitude or EC_{50} (Fig. 4A,B), GABA-evoked currents were significantly reduced in C9orf72 neurons without changes in EC_{50} values, suggesting impaired inhibitory signaling without altered receptor sensitivity (Fig. 4C,D).

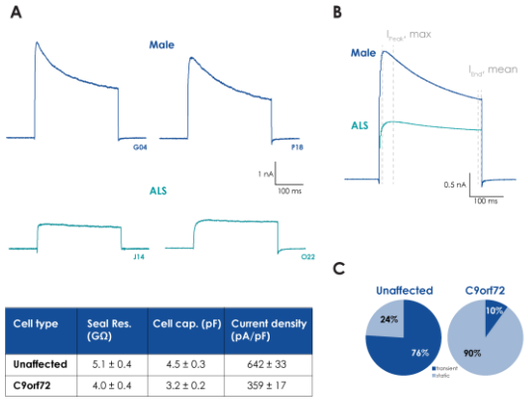

Cell type	Seal Res. (GΩ)	Cell cap. (pF)	Current density (pA/pF)
Unaffected	5.1 ± 0.4	4.5 ± 0.3	642 ± 33
C9orf72	4.0 ± 0.4	3.2 ± 0.2	359 ± 17

Figure 3: A Potassium (K^+) currents from unaffected and C9orf72 motor neurons were recorded using a voltage step protocol to 60 mV, revealing distinct waveform morphologies. Unaffected neurons showed fast activation with pronounced inactivation, whereas C9orf72 neurons displayed sustained currents with little or no inactivation. C9orf72 motor neurons exhibited significantly reduced current amplitudes, slightly lower capacitance, and a markedly decreased current density compared with unaffected neurons (Table). **B** Average traces for unaffected and ALS K_V currents shown overlaid. **C** Analysis of waveform distribution revealed a significant shift from transient to monotonic K+ current decay in C9orf72 motor neurons.

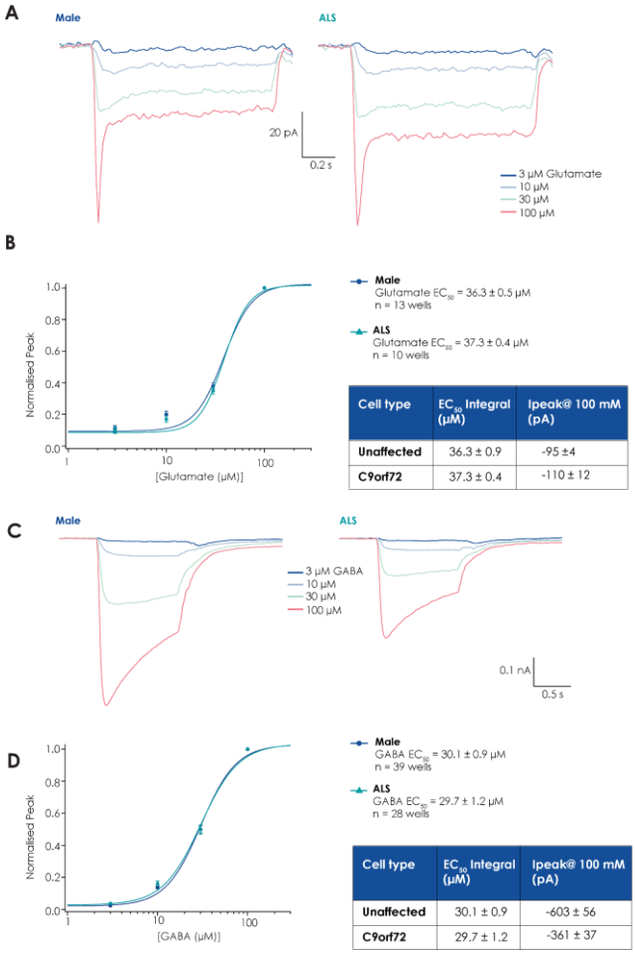

Cell type	EC_{50} Integral (µM)	Ipeak@ 100 mM (pA)
Unaffected	36.3 ± 0.9	-95 ±4
C9orf72	37.3 ± 0.4	-110 ± 12

Cell type	EC_{50} Integral (µM)	Ipeak@ 100 mM (pA)
Unaffected	30.1 ± 0.9	-603 ± 56
C9orf72	29.7 ± 1.2	-361 ± 37

Figure 4: Neurotransmitter response - Glutamate. No differences were observed between unaffected and C9orf72 motor neurons in **A** current amplitude or **B** EC_{50} values for glutamate responses; glycine responses were also unchanged (not shown). Neurotransmitter response - GABA. **C** GABA-evoked current amplitudes differed between unaffected and C9orf72 motor neurons, while **D** EC_{50} values were comparable between groups.

Conclusion

iPSC-derived motor neurons are a physiologically relevant ALS model, preserving patient genetics and enabling functional phenotyping. Automated patch clamp was used to robustly characterize C9orf72 neurons, confirming disease-relevant changes. These included altered morphology consistent with cytoskeletal dysfunction. APC revealed remodelled K^+ currents, reduced Na^+ currents, and impaired inhibitory (GABA) signalling, while glutamate and glycine responses were unchanged. High data quality and throughput support scalable, disease-relevant drug discovery and ion channel screening, even beyond the ALS phenotype.

A human cell-based atrial fibrillation disease model

Bettina Lickiss, Jan Hunker, Britta Simons, Peter Linder, Matthias Gossmann
innoVitro GmbH, Juelich, Germany

Abstract

Atrial fibrillation (AF) is the most common form of cardiac arrhythmia, significantly impacting morbidity and mortality worldwide. Using commercially available human induced pluripotent stem cell (hiPSC)-derived atrial cardiomyocytes (axoCells™, Axol Bioscience Ltd.) (Lickiss & Hunker et al., 2024), we developed an AF-like human phenotype in vitro disease model based on the protocol of Seibertz et al., 2022. The drug screening assay is designed to assess AF-related functional changes in a human-relevant context, with extracellular field potential duration (EFP duration, CardioExcyte 96, similar to MEA) as readout parameter.

Figure 1A

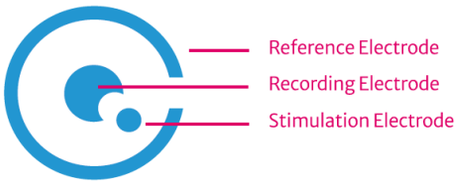

Figure 1B

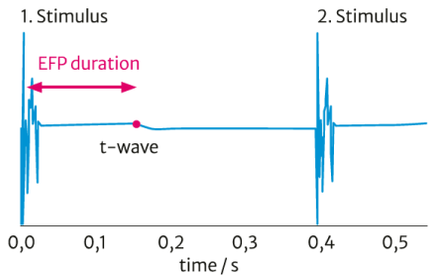

Figure 1A. Well design of a CardioExcyte 96 plate containing a reference electrode (outer ring), a recording electrode (placed in the middle) and a stimulation electrode for performing electrical pacing on cells. Figure 1B. Schematic view of EFP duration analysis between two stimuli using a raw data example.

Figure 2

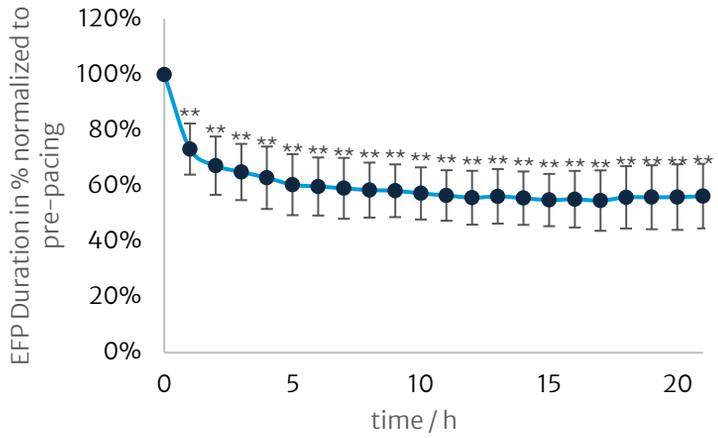

Figure 2. Effect of 2.5 Hz tachypacing on atrial hiPSC-CMs. Cells were electrically paced for 24h showing a 40% decrease in EFP duration after approx. 5 h (n=50) that remained stable throughout tachypacing. Statistical analysis performed with Wilcoxon-Mann-Whitney (WMW) test.

Methods

Preculture of atrial hiPSC-CMs on CardioExcyte 96 plates (Figure 1A) for 9 days including medium changes every other day. Begin of tachypacing in CardioExcyte 96 device on day 9 for 24 h -> induction of electrical remodelling (AF phenotype) shown by reduced EFP duration (Figure 2). Compound addition 24 h after begin of tachypacing followed by chronic EFP duration assessment (Figure 1B).

Results

Figure 3

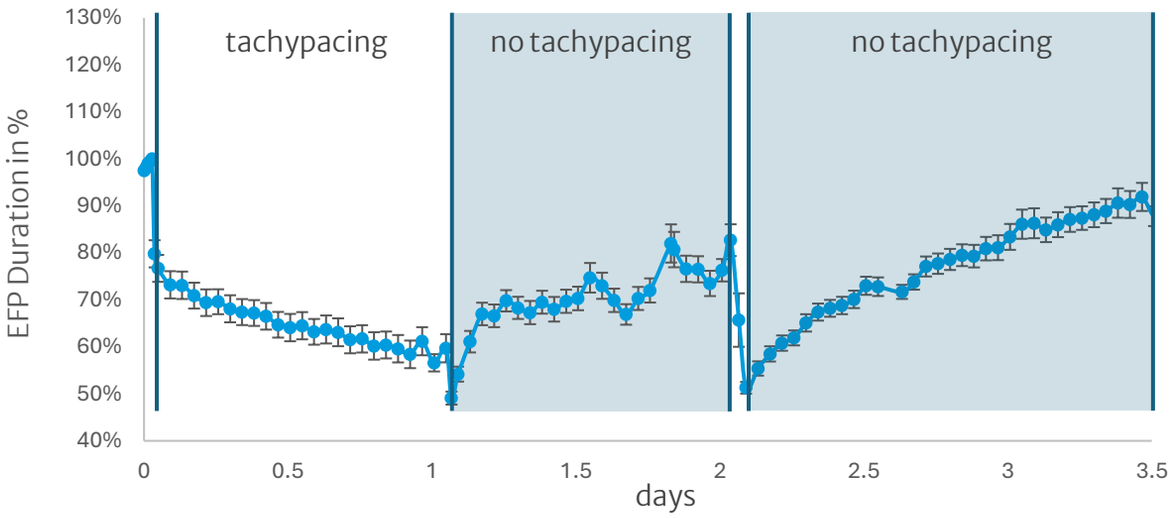

Figure 3. Effect of 2.5 Hz tachypacing on EFP duration of atrial hiPSC-CMs. Chronic tachypacing leads to a 40% shortening in EFP duration over 24 h, while stop of pacing shows a slow normalization of EFP duration towards pre-tachypacing condition.

Tachypacing of atrial hiPSC-CMs induced electrical remodeling, evidenced by a significant shortening of EFP duration, corresponding to QT interval shortening (Figure 2). Upon cessation of tachypacing, cells exhibited gradual recovery, with EFP duration increasing from ~55% to ~80% and ~ 90% respectively over 24 hours (Figure 3).
S-bay treatment induced a dose-dependent prolongation of EFP duration in atrial hiPSC-CMs. This effect was fully reversible upon washout (Figure 4), demonstrating the reversible/rescue effects that can be tested using this human-based AF approach.

Figure 4

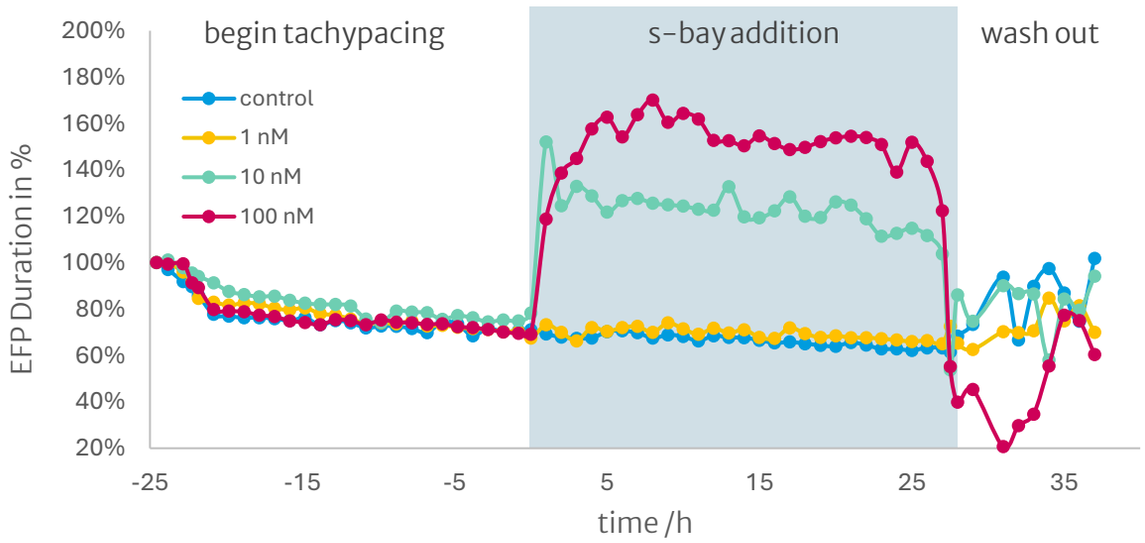

Figure 4. Effect of s-bay on atrial hiPSC-CMs under 2.5 Hz tachypacing condition. Cells show a dose-dependent increase in EFP duration after s-bay addition and a a decrease after wash out of the compound, while control condition remains stable around 60% under ongoing tachypacing.

Conclusion

This human-based disease model presents a significant advancement for AF research, providing a human-relevant platform for identifying novel therapies with greater translational potential and accelerating the development of effective AF treatments.

References

Lickiss & Hunker et al., 2024. Chamber-specific contractile responses of atrial and ventricular hiPSC-cardiomyocytes to GPCR and ion channel targeting compounds: A microphysiological system for cardiac drug development. Vol 128, JPTM.

Seibertz et al., 2022. Atrial fibrillation-associated electrical remodelling in human induced pluripotent stem cell-derived atrial cardiomyocytes: a novel pathway for antiarrhythmic therapy development. Vol 119, Cardiovascular Research.

SOPHION BIOSCIENCE | Discover more

High-throughput electrophysiological characterization and screening of ventricular axoCells™ cardiomyocytes, using Sophion's APC platforms QPatch and Qube 384

Atanaska Velichkova, Kadla R. Rosholm
Sophion, Ballerup, Denmark

Abstract

Automated patch clamp (APC) systems enable high-throughput, precise electrophysiological measurements of cardiac ion channels in human induced pluripotent stem-cell derived cardiomyocytes
(hiPSC-CMs), accelerating screening workflows of these key therapeutic and safety targets.

This study employs Sophion QPatch and Qube 384 APC platforms (figure 1) to biophysically and pharmacologically evaluate cardiac ion channels ($Na_v1.5$ and $Ca_v1.2$) and paced action potentials in axoCells™ ventricular hiPSC-CMs, highlighting the potential of this technology in cardiac safety and drug-discovery.

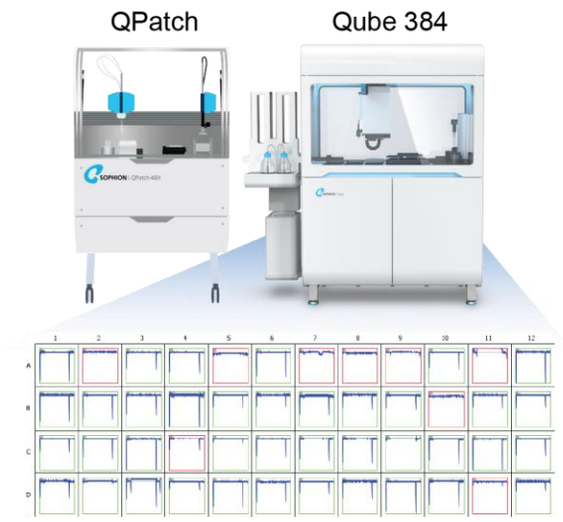

Figure 1: Sophion APC platforms QPatch (left) and Qube 384 (right) including the Qube plate view (48 out of 384 experiment sites) displaying Na_v currents recorded in axoCells™ hiPSC-CMs

Biophysical characterization and screening of $Na_v1.5$ on Qube 384

Using customized dissociation and whole-cell protocols we obtained a good-quality single-cardiomyocyte suspension that could be recorded on Qube 384 with up to 80 % success rates (figure 2A). First, we did a biophysical characterization of $Na_v1.5$, with the current-voltage relationship and V_{half} of activation and inactivation in good agreement with literature values (figure 2B-E).

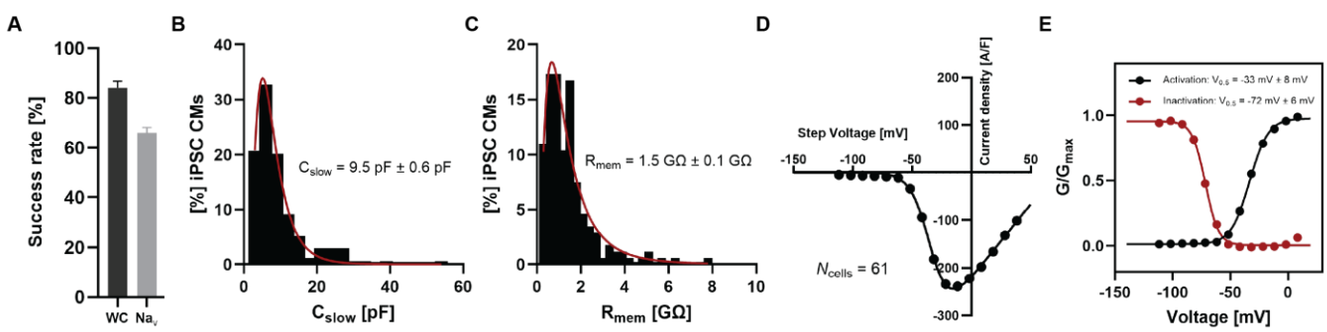

Figure 2: Performance of axoCells™ hiPSC-CMs on Qube 384. A) experiment success rates plotted for whole-cell (WC) and Na_v current in percentage of experiment sites. **B)** and **C)** Histograms of C_{slow} and R_{mem} values of the measured cell population (N_{cells} = 177) and best fit of the distribution (red line). **D)** Na_v current density vs. step voltage plot. Data points are mean ± SEM of 61 cells. **E)** Normalized conductance vs voltage plotted for Na_v activation (black) and inactivation (red). Fit of the Boltzmann equation resulted in a $V_{half,act}$ and $V_{half,inact}$ of approximately – 33 mV and -72 mV, respectively, in line with reported values for Nav1.5.

The good experiment success rate and data quality allow us to do a sample $Na_v1.5$ compound concentration-response experiment using the well-known state-dependent Na_v blocker, tetracaine (figure 3).

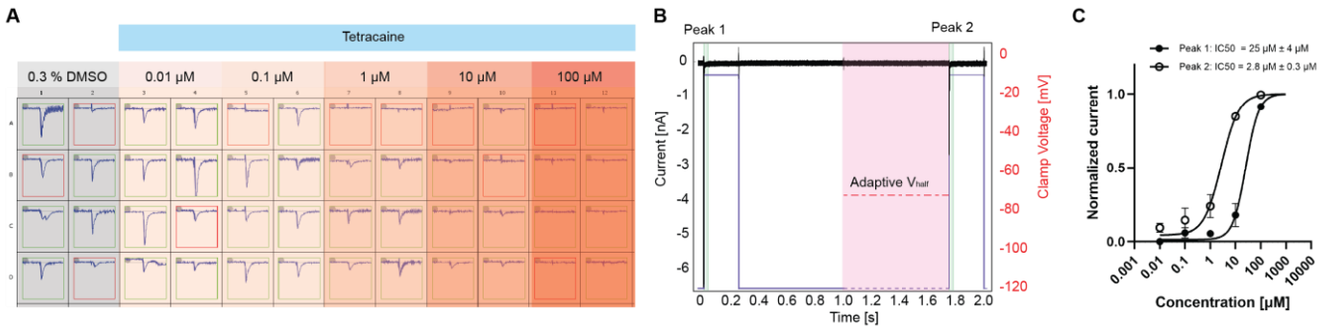

Figure 3: Na_v blocker concentration-response experiment using axoCells™ hiPSC-CMs on Qube 384. A) Plate view (48 out of 384 experiment sites) displaying Na_v peak currents recorded in hiPSC-CMs upon the addition of 0.3 % DMSO (control, grey) or increasing concentrations of the state-dependent Na_v blocker tetracaine (5 point 10-fold dilution from 100 µM, orange). **B)** The two-pulse protocol used to evaluate the state-dependent blocker, consisting of two 0.2 s pulses, from -120 mV to -10 mV, separated by 1.6 s in total, 0.8 s at -120 mV and 0.8 s at the V_{half} value recorded adaptively for each single cell. **C)** Normalized Na_v peak current as a function of tetracaine concentration plotted for peak 1 (solid black) and peak 2 (black outline), respectively. Fitting of the Hill equation resulted in IC50 values of approximately 25 µM and 2.8 µM, for peak 1 and peak 2 respectively, in line with previous studies.

Recording and compound modulation of $Ca_v1.2$ and action potentials in physiological solutions on QPatch

We recorded L-type $Ca_v1.2$ channel currents and paced action potentials (APs) in about 60 % of the axoCells™ hiPSC-CMs using physiological solutions on QPatch (figure 4). As expected, the APs were significantly prolonged when the $Ca_v1.2$ current was potentiated and shortened when the $Ca_v1.2$ current was blocked.

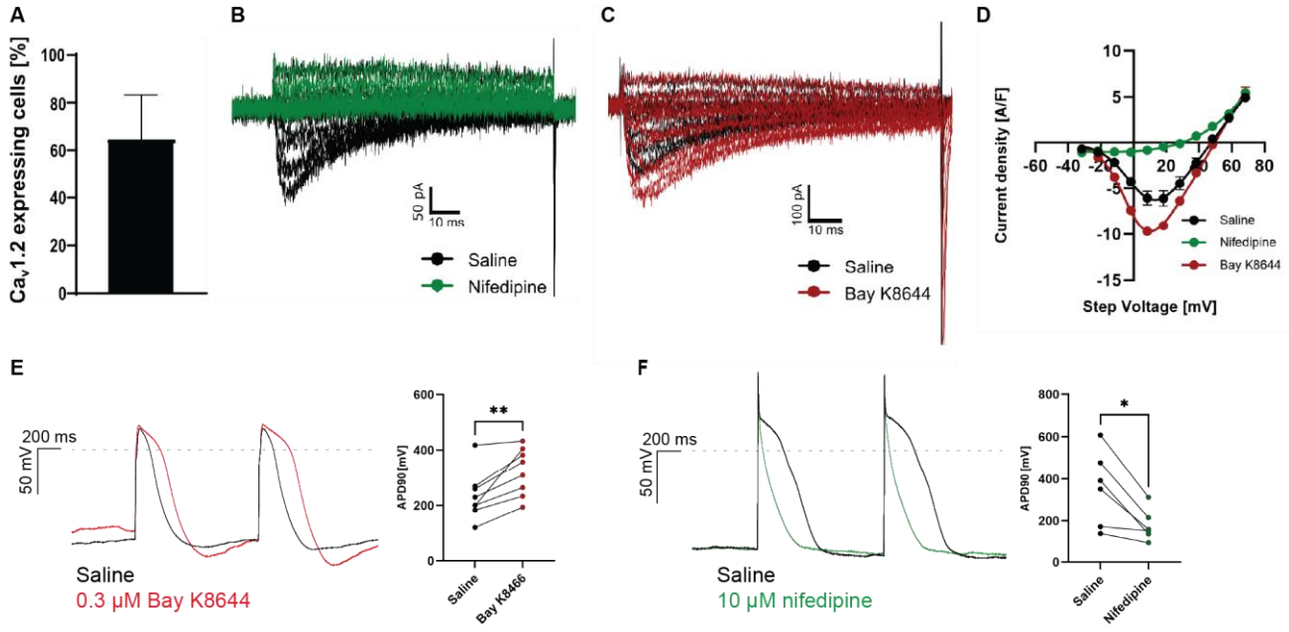

Figure 4: Recordings of $Ca_v1.2$ currents and paced action potentials in axoCells™ hiPSC-CMs on QPatch. A) Percentage of successful experiments with Ca_v current. Data is mean ± SEM of three experiment plates. **B)** Representative Ca_v current trace in response to a voltage step protocol before (black) and after (green) addition an L-type Cav channel blocker (10 µM nifedipine). **C)** Representative Ca_v current trace in response to a voltage step protocol before (black) and after (red) addition of an L-type Ca_v channel agonist (0.3 µM bay K8644). **D)** Ca_v current density vs. step voltage plot recorded in saline (black), 10 µM nifedipine (green) and 0.3 µM bay K8644 (red). Data points are mean ± SEM of 7 – 10 cells. Below, we display paced APs and plot of APD90 values before (control, black traces and data points) and after addition of: **E)** 10 µM nifedipine (green trace and data) and **F)** 0.3 µM Bay K8644 (red trace and data). The statistical comparison was performed with a paired t-test, $p < 0.05$ (*) and $p < 0.01$ (**).

Thank you to our collaborators who are working on breaking new ground in new approach methodologies

Optics11 Life - A highly reproducible and precise measurement platform for 3D engineered cardiac muscle tissue contractility

3Brain - Functional profiling of human iPSC-derived neuronal networks with 3Brain's CorePlate™ HD-MEA technology

Nanion - Profiling ALS variants and ion channel expression changes with HT automated patch clamp

innoVitro - A human cell-based atrial fibrillation disease model

Sophion - High-throughput electrophysiological characterization and screening of ventricular axoCells™ cardiomyocytes, using Sophion's APC platforms QPatch and Qube 384

LRQA CERTIFIED ISO 9001

UKAS MANAGEMENT SYSTEMS 0001

Quality manufacturing
We manufacture iPSC-derived cell types at our ISO 9001:2015 production facility.

Global logistics
We supply our products worldwide to pharma, biotech, research and technology providers.

Dedicated team
With a highly skilled, science-led team, we work collaboratively to generate more predictive models of human biology and disease.

www.axolbio.com
operations@axolbio.com